JACS
JOURNAL OF THE AMERICAN CHEMICAL SOCIETY
Article
pubs.acs.org/JACS

Control of Electronic Symmetry and Rectification through Energy Level Variations in Bilayer Molecular Junctions

Akhtar Bayat,[†] Jean-Christophe Lacroix,[‡] and Richard L. McCreery*[,†,§]

[†]University of Alberta, 11421 Saskatchewan Drive, Edmonton, Alberta T6G 2M9, Canada

[‡]Université Paris Diderot, Sorbonne Paris Cité, ITODYS, UMR 7086 CNRS, 15 rue Jean-Antoine de Baïf, 75205 Paris Cedex 13, France

[§]National Institute for Nanotechnology, 11421 Saskatchewan Drive, Edmonton, Alberta T6G 2M9, Canada

Supporting Information

ABSTRACT: Two layers of molecular oligomers were deposited on flat carbon electrode surfaces by electrochemical reduction of diazonium reagents, then a top contact applied to complete a solid-state molecular junction containing a molecular bilayer. The structures and energy levels of the molecular layers included donor molecules with relatively high energy occupied orbitals and acceptors with low energy unoccupied orbitals. When the energy levels of the two molecular layers were similar, the device had electronic characteristics similar to a thick layer of a single molecule, but if the energy levels differed, the current voltage behavior exhibited pronounced rectification. Higher current was observed when the acceptor molecule was biased negatively in eight different bilayer combinations, and the direction of rectification was reversed if the molecular layers were also reversed. Rectification persisted at very low temperature (7 K), and was activationless between 7 and 100 K. The results are a clear example of a "molecular signature" in which electronic behavior is directly affected by molecular structure and orbital energies. The rectification mechanism is discussed, and may provide a basis for rational design of electronic properties by variation of molecular structure.

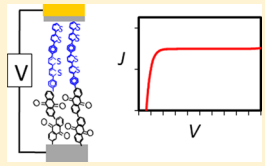

INTRODUCTION

Charge transport in solid state molecular films has stimulated major research efforts, with one goal being manipulation of electronic behaviors by changes in molecular structure. For monomolecular layers or oligomers of organic molecules with thickness of 1−20 nm, transport properties differ significantly from those in thicker films, and such devices are considered "molecular electronics".[1−4] The basic component of molecular electronics is a "molecular junction (MJ)" consisting of a single molecule or an ensemble of many molecules oriented in parallel between two conducting contacts. Quantum mechanical tunneling and possibly ballistic transport distinguish molecular electronics from the widely studied "organic electronics" in which transport occurs by a series of steps, often mediated by redox exchange. A wealth of results for molecular layers with thickness, d, in the range d = <1−3 nm strongly support tunneling as the dominant mechanism for transport in aliphatic MJs, exhibiting an exponential decrease in junction current with increasing distance.[4−8] The attenuation factor, β, for the exponential decay is in the range of 7−9 nm^{-1} for alkane MJs, comparable to that observed for electron transport through similar layers to redox systems in electrolyte solution.[9−14] MJs based on alkanes exhibit a range of electronic properties, including rectification[15−19] and inelastic tunneling,[20−23] but transport is generally limited by the high β value to a few nanometers.

Transport in conjugated molecular layers differs fundamentally from that in alkanes, due mainly to extended delocalization of orbitals across distances which might be comparable to the MJ thickness. Although the dependence of MJ current on d is often exponential, β is much smaller than observed for alkanes, in the range of <0.1 to 5 nm^{-1}, with the most commonly reported examples close to 3 nm^{-1}.[3,4,24−26] Conjugated MJs also exhibit strong electronic coupling between the contacts and the molecules, resulting in a "compression" of tunneling barriers attributed to electrostatic effects of partial charge transfer across the contact/molecule interface.[27−32] Strong coupling can decrease the effects of structural changes on transport for molecular layers in the range of d = 1−5 nm, thus significantly modifying the energy levels of transport orbitals relative to those of the free molecules. Some conjugated MJs also exhibit a change in β for d in the range of 3−8 nm, attributed to an alternative mechanism to tunneling such as redox "hopping".[24,25,29] For the case of bisthienylbenzene (BTB) molecular layers up to d = 22 nm, activationless transport was observed with a $\beta \approx 1$ nm^{-1} at temperatures below 10 K, and high current densities (>10 A/cm^2) were possible without apparent MJ damage.[33] These observations clearly indicate unusual transport mechanisms for conjugated MJs with d in the range of 5−22 nm, which are consistent neither with coherent tunneling nor with activated "hopping" mechanisms based on redox exchange.[3]

Most conjugated MJs reported to date have contained a single molecular structure, either as a monolayer or as oligomers with a range of molecular lengths. In most cases with a single molecular layer between two electrodes of the same material, the current-density vs bias voltage (JV) behavior

Received: July 20, 2016
Published: August 26, 2016

DOI: 10.1021/jacs.6b07499
J. Am. Chem. Soc. 2016, 138, 12287−12296

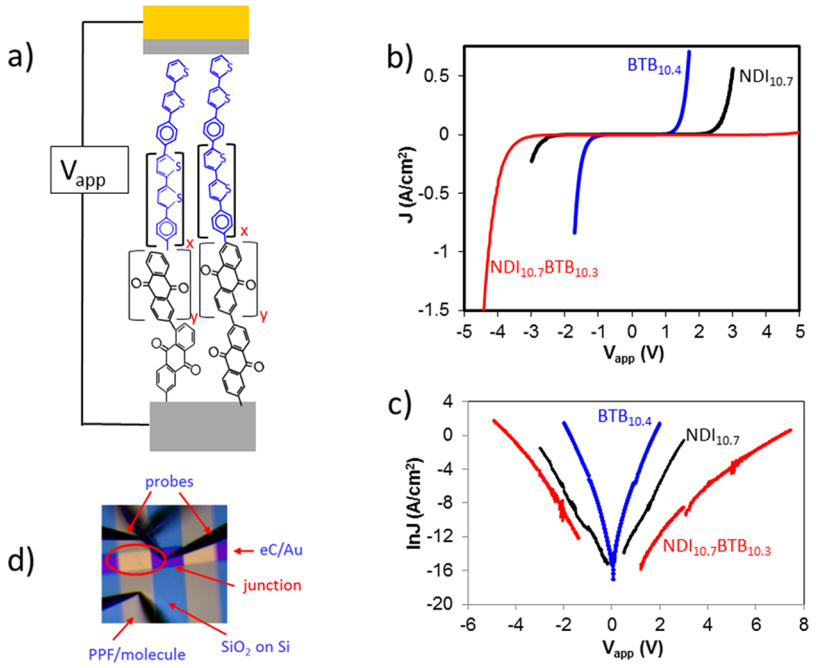

Figure 1. (a) Schematic illustration of a bilayer molecular junction with an initial layer of anthraquinone (AQ) on pyrolyzed photoresist film (PPF) followed by a second layer of bis-thienyl benzene (BTB). *x* and *y* indicate varying lengths of oligomers. (b) Current density vs bias voltage (*JV*) curves of NDI/BTB, NDI-only and BTB-only junctions, obtained in vacuum at 1000 V/s. (c) Same *JV* curves plotted as ln *J* vs *V*. *JV* curves shown in all figures are averages of 4 molecular junctions. (d) Image of 250 μm × 500 μm junction, showing tungsten probe tips.

is symmetric with respect to polarity, for example in Au/oligophenylimine/Au MJs[28,29,34] and a variety of aromatic structures between conducting carbon electrodes,[3,26,27] including the aforementioned BTB oligomer layers with d = 4−22 nm.[33] While the current paper is directed toward understanding how energy levels affect transport, there is significant literature on "molecular rectifiers", starting with an early theoretical proposal by Aviram and Ratner[35] based on donor and acceptor molecules separated by an aliphatic bridge. Decades of research on rectification by single molecules or ensembles of many molecules in parallel between two conductors was reviewed recently,[2] with the donor/acceptor mechanism prominent, in which unidirectional charge transport is favored from the relatively high energy HOMO of the donor to the LUMO of the acceptor.[36−38] A different mechanism observed in alkyl-Ferrocene self-assembled monolayers involves differences in transport mechanisms through the Fc and alkane orbitals, and is strongly dependent upon the position of the Fc between the two conducting surfaces.[15,17,39,40] Several other mechanisms for molecular rectification have been reported, including asymmetric contacts,[41−45] ionic screening or transport,[46,47] contact roughness differences,[48] and molecular layers on silicon.[49−53] There are also many reports about "organic p-n diodes" composed of >100 nm thick films of organic donor and acceptor molecules,[54−59] but the current report discusses much thinner molecular layers, i.e., < 20 nm, with different transport mechanisms as described below.

Our group used a carbon/molecule/carbon MJ structure to examine molecular bilayers made with "click" chemistry and d < 5 nm, in order to introduce structural asymmetry into the MJ interior.[60] Bilayers containing ethynylbenzene and Fc or aliphatic molecules did not show *JV* asymmetry and β was consistently ∼2.8 nm^{-1}, despite a variety of molecular structures in the "click" portion of the molecular layer. We proposed that the differences in molecular structure and orbital energies in the bilayer were "washed out" by strong electronic coupling and the majority aromatic composition of the MJ.[27,60] This result, combined with the changes in transport mechanism observed above 5 nm in BTB based junctions,[32] stimulated consideration of bilayers with thicknesses totalling more than 5 nm, to explore the possibility that strong coupling would not extend across the entire junction and molecular orbital energies would more strongly affect transport. The current report describes bilayer MJs made by successive electrochemical reduction of two different diazonium reagents, yielding bilayer thicknesses of 10−20 nm, shown schematically in Figure 1a. The contacts were both disordered sp^2 carbon, so compositional asymmetry was present only in the molecular layer. Recent reports on carbon/carbon MJs with a single molecular structure show symmetric *JV* behavior over the entire range of <4 to 22 nm, and this symmetry is consistent for at least four distinct oligomer structures.[33,61] By varying the composition of the two molecular layers, the effects of molecular orbital energies on *JV* symmetry were observed, and represent a "molecular signature" demonstrating structural effects on electronic behavior.

EXPERIMENTAL SECTION

MJs were fabricated using a pyrolyzed photoresist film (PPF) substrate and an electron beam deposited carbon (eC) top contact as described in detail previously,[62] with lateral dimensions of 250 by 500 μm (area = 0.00125 cm^2). The work function of PPF was determined by Ultraviolet Photoelectron Spectroscopy (UPS)[27] for five different PPF preparations made on different days and analyzed within 2 h of pyrolysis, yielding a value of −4.7 ± 0.1 eV relative to vacuum. With the exception of bis-thienyl benzene (BTB), diazonium reagents were synthesized and isolated as fluoroborate salts for 2-anthraquinone (AQ), fluorene (FL), nitroazobenzene (NAB) and a derivative of phenyl naphthalene di-imide[63] (NDI). Molecular structures of the aromatic amine precursors are shown in SI, Figure S1. The fluoroborate salt of BTB could not be isolated, hence it was prepared

DOI: 10.1021/jacs.6b07499
J. Am. Chem. Soc. 2016, 138, 12287−12296

in situ before electrochemical deposition by previously reported procedures.[33,42,64] Molecular bilayers were deposited by successive electrochemical reduction of different aromatic diazonium precursors,[65] with voltammetric parameters determined empirically. Table S1 of Supporting Information (SI) lists the electrochemical conditions for all the bilayers reported herein and the resulting layer thicknesses. Molecular layer thicknesses were determined by AFM "scratching" of a region adjacent to the molecular junctions,[66] using a statistically well-defined procedure,[33] with an example shown in SI Figure S2. For bilayer devices, the AFM thickness was determined before and after deposition of the second layer, and the second layer thickness was obtained by difference. Standard deviations of thickness were in the range of 0.4 to 0.8 nm as indicated in Table S1. The very thin junction layers prevented detailed characterization by optical spectroscopy, but one example for molecules with sufficient UV−vis absorption (AQ and BTB) is shown in Figure S3 of SI. Comparison of the single layer absorption with that of the bilayer showed that the layer absorbances are approximately additive, indicating that the chromophores of the two molecules are not significantly altered by formation of the bilayer. X-ray photoelectron spectroscopy of PPF/NDI surfaces before and after BTB deposition are provided in SI, Figure S4 and Table S2. The O_{1s} peak from the imide oxygen of NDI decreases in coverage from 7.4 atom % to ∼1.3 atom % upon BTB deposition, and the S_{2p} feature from BTB increases from 0 to 9.3 atom %. PFF/NDI exhibits an imide N_{1s} peak at 400.5 eV and 4 atom % coverage, which decreases to near zero upon BTB deposition. A small azo N_{1s} feature at 399.5 eV appears after BTB deposition, presumably due to a small amount of azo coupling which occurs in many diazonium-derived films.[67−69] Junction designations include subscripts indicating layer thicknesses in nanometers, with all devices using a ∼1 μm thick PPF substrate and top contact of 10 nm of electron beam carbon and 30 nm of electron beam deposited Au. For example, $PPF/AQ_{10}BTB_8/eC_{10}/Au_{30}$ indicates a bilayer of 10 nm of AQ and 8 nm of BTB formed electrochemically on PPF, then the eC/Au top contact deposited in vacuum, as described previously.[62] In all cases, the PPF/molecule/eC_{10}/Au_{30} junction structure was used.

Completed molecular junctions were tested initially in air with a Keithley 2602A source-measurement unit or LabVIEW-based scanning instruments.[70,71] The resulting current-density/voltage (*JV*) curves exhibited hysteresis and scan rate dependence when acquired in air (shown in Figure S5a), implying changes in junction structure and/or behavior with application of bias scans. In vacuum ($<1 \times 10^{-5}$ Torr for several hours), these effects were absent, as shown in Figure S5b. The dynamic properties are likely due to unintended redox reactions involving residual water, and could be reduced or avoided in a vacuum. For this reason, all MJs discussed below were transferred from the electron beam deposition chamber ($<1 \times 10^{-6}$ Torr) to a vacuum probe station ($<1 \times 10^{-4}$ Torr) with no intervening application of a bias and minimal air exposure. As shown below, vacuum operation combined with fast voltammetric scans eliminated hysteresis and also prolonged junction lifetime, with randomly selected junctions showing minor changes in *JV* response after >10 000 scans in vacuum. All *JV* curves in figures were obtained in vacuum with a scan rate of 1000 V/s, and each curve presented in figures is an average of at least four MJs. The standard deviations of *J* and RR for 55 MJs and eight bilayer combinations are provided in Table 1 below, and representative *JV* curves with error bars are provided in SI figure S6.

RESULTS

The carbon/oligomer/carbon junction structure shown in Figure 1a and described in detail previously[26,27,33,62] is characterized by covalent, conjugated bonding both between the PPF contact and the molecular oligomer and within the molecular layer. While the molecular orientation is largely perpendicular to the PPF substrate,[72] it has a range of dihedral angles between molecular subunits, as well as variation in the geometry of the intermolecular linkages. Current-density vs applied voltage (*JV*) curves for MJs containing only one molecular subunit are shown in Figure 1b, for the case of ∼10.5 nm thick films of BTB and NDI. As reported previously, *JV* curves for junctions containing only one molecular component are symmetric with respect to polarity, and differ significantly in current magnitude provided the thickness, *d*, is greater than 6 nm.[33,61] As shown in Table 1, the calculated HOMO and LUMO energies for the free molecular monomers of BTB and NDI differ significantly, with the relatively high energy of the BTB HOMO (−5.29 vs. vacuum) making it an electron donor, and the low LUMO energy of NDI (- 3.35 eV) making it an acceptor. The Fermi level of PPF is assumed to equal the work function determined by UPS (−4.7 ± 0.1 eV vs vacuum), and the offset between the molecular orbitals and the contact Fermi level is often used to estimate the tunneling barriers for MJs.[27] Notice that the BTB and NDI current densities differ by two to 3 orders of magnitude for the ∼10.5 nm films, depending on bias, similar to the difference observed for 7−8 nm thick devices,[61] but much larger than that exhibited in 2−5 nm MJs.[27] Figure 1b also shows the *JV* response for a bilayer made by successive reduction of BTB and NDI diazonium precursors, yielding a thickness comparable to the sum of the two individual layers. The current density decreases significantly for the thicker bilayer film, but very asymmetrically with respect to polarity. The logarithmic plot of Figure 1c shows that the asymmetry is present over a wide bias range from <2 to 5 V. The absolute value of the ratio of the current for negative bias to that for positive bias of the same voltage, often defined as the rectification ratio (RR) increases from ∼82 at ±3.5 V to 190 at ±4.5 V for the NDI/BTB bilayer. Unless stated otherwise, the rectification ratios were determined at the bias where either the negative or positive current density reaches 0.2 A/cm^2. Comparable values for either BTB or NDI alone are less than 2.0 over the entire voltage range shown in Figure 1, and up to higher bias for thicker films (see Figure S7a). The pronounced asymmetry observed for NDI/BTB devices compared to NDI alone provides good evidence that the eC top electrode is not penetrating the BTB layer.

As noted previously, a feature of diazonium-derived organic films is the ability to vary thickness of the molecular layers by changing the deposition conditions. Figure 2a shows *JV* curves for several BTB thicknesses deposited as a second layer on an initial layer of 13.5 nm NDI, and Figure 2b is the same data on a logarithmic scale. A 2 nm BTB layer has little effect on *JV* symmetry, with a RR < 2 at ±3.6 V, but a 6 nm BTB layer shows rectification, with RR = 25 at ±3.9 V. The effect of BTB thickness is asymmetric with respect to bias, and may be visualized as a plot of ln *J* vs BTB layer thickness, analogous to the "*β*" plots often presented for single-layer molecular junctions. Figure 2c shows such plots of ln *J* vs BTB thickness

Table 1. Calculated Orbital Energies from Density Functional Theory[a]

	free molecules		dimers	
	HOMO (eV)	LUMO (eV)	HOMO (eV)	LUMO (eV)
BTB	−5.29	−1.48	−4.99	−1.93
NDI	−6.92	−3.35	−6.41	−3.38
AQ	−7.00	−2.77	−6.83	−3.03
FL	−5.75	−0.71	−5.31	−1.18
NAB	−6.66	−3.04	−6.61	−3.64

[a]B3LYP 6-31G(d), in Gaussian 09. This procedure often yields higher LUMO energies and HOMO−LUMO gaps than observed experimentally, so the LUMOs should be considered approximate.

DOI: 10.1021/jacs.6b07499
J. Am. Chem. Soc. 2016, 138, 12287−12296

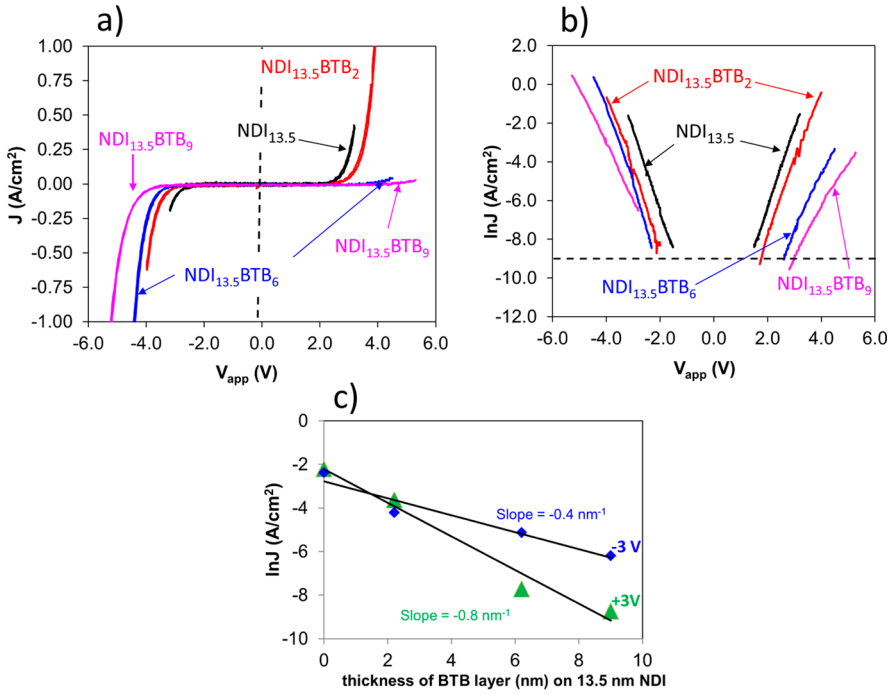

Figure 2. (a) Overlay of *JV* curves of a series of bilayers with constant NDI thickness and increasing BTB thickness as indicated. (b) Overlay of ln *J* vs *V* curves for the same devices. (c) Plots of ln *J* versus the BTB thickness measured at ±3 V. Slopes indicate the attenuation coefficient for the BTB layer.

Table 2. Rectification Ratios for NDI and BTB Single Component MJs and NDI-BTB Bilayers

	first layer thickness, nm	second layer thickness,[a] nm	total thickness, nm	V_1 for $\|J\|$ = 0.2 A/cm^2	$J(-V_1)$	$J(+V_1)$	RR ($\pm V_1$)
NDI	13.5	0	13.5	−3.2	−0.195	0.391	0.50
NDI	10.7	0	10.7	−2.96	−0.208	0.484	0.43
NDI	4.1	0	4.1	−0.27	−0.204	0.188	1.09
NDI	23.9	0	23.9	6	−0.064	0.182	0.35
BTB	10.4	0	10.4	−1.47	−0.202	0.157	1.29
BTB	22	0	22.2	−3.63	−0.210	0.483	0.43
NDI/BTB	13.5	2	15.7	−3.59	−0.212	0.264	0.80
NDI/BTB	13.5	6	19.7	−3.92	−0.203	0.008	25.0
NDI/BTB	3.8	6.5	10.3	−1.97	−0.212	0.199	1.06
NDI/BTB	4.1	9.2	13.3	−2.58	−0.199	0.061	3.27
NDI/BTB	13.5	9	22.5	−4.53	−0.208	0.006	34.8
NDI/BTB	10.7	10.3	21	−3.92	−0.207	0.003	80

[a]Determined by difference between total and first layer thicknesses.

at +3 and −3 V, with a constant thickness of 13.5 nm of NDI. The slopes are 0.4 nm^{-1} at −3 V and 0.8 nm^{-1} at +3 V, with the higher value corresponding to the greater attenuation of *J* with BTB thickness at positive bias. Table 2 lists the rectification ratios for various single layer and bilayer MJs, and the largest RR values were observed for bilayers with both components having layer thicknesses of ∼10 nm. As shown in Figure S8, an NDI layer thinner than 10 nm produced weak rectification, similar to the case for thin BTB layers on $NDI_{13.5}$. Although the difficulty of fabrication of bilayers with controlled thickness made a systematic study difficult, the remaining bilayer devices had approximately equal thicknesses of both components, in the range of 8−14 nm.

To test the role of orbital energies on *JV* symmetry, NDI-AQ bilayers were compared to NDI-BTB. As noted above, NDI and BTB have quite different calculated HOMO and LUMO energies, with NDI considered an acceptor and BTB a donor. The orbital energies depend on the length of the oligomers, with the HOMO−LUMO difference decreasing for longer molecules,[26] and Table 1 includes energies for both monomers and dimers. Using the dimers as approximations of the oligomer energies, the HOMO energies for BTB and NDI differ by 1.42 eV, while the LUMOs differ by 1.45 eV. In contrast, AQ and NDI are both acceptors, with their dimer HOMOs differing by 0.42 eV and LUMOs by 0.35 eV. These differences are more easily visualized in the energy diagrams of Figure 3a and 3b, which assume an electrode Fermi level of −4.7 V vs vacuum.

Although electronic coupling between the oligomers and the contacts as well as between bilayers is likely significant and may affect orbital energies, the schematics of Figure 3a and 3b provide some guidance regarding orbital energy differences. Figure 3c is an overlay of the NDI/BTB results of Figures 1 and 2 for two thicknesses of each molecular layer, each showing significantly higher currents for negative bias and RR of 35 and 80 as listed in Table 2. The RR typically increases with bias, e.g.

DOI: 10.1021/jacs.6b07499
J. Am. Chem. Soc. 2016, 138, 12287−12296

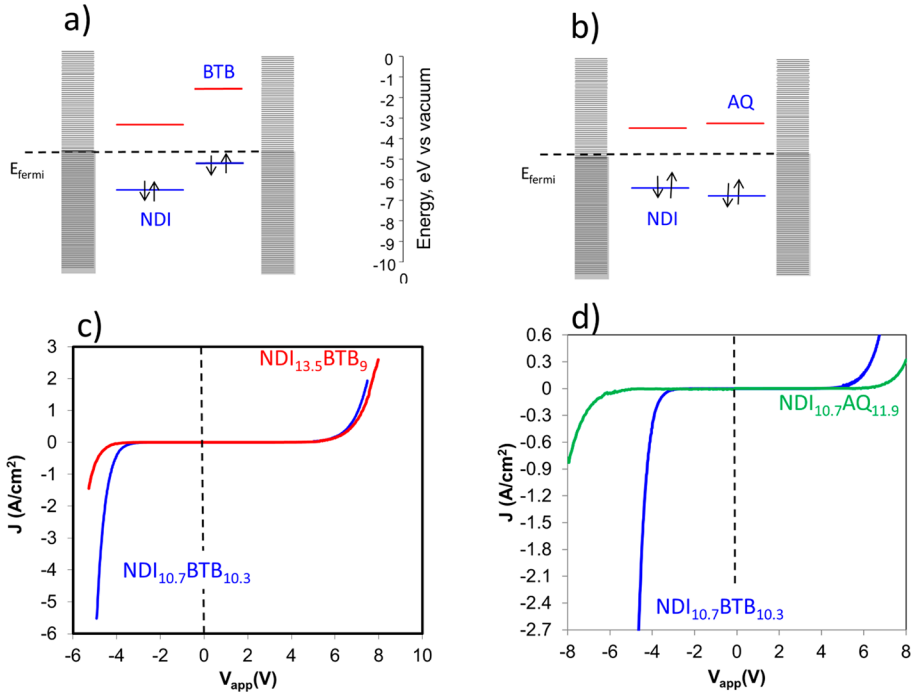

Figure 3. Energy level diagrams for (a) NDI-BTB, and (b) NDI-AQ bilayers, based on free-molecule DFT energies for the HOMO (blue) and LUMO (red) at zero bias. (c) *JV* curves for NDI-BTB rectifiers with slightly different thicknesses. Note the significant asymmetry relative to $V = 0$ (dotted line). (d) *JV* curve of NDI-BTB rectifying bilayer compared to symmetric *JV* curve of NDI-AQ bilayer.

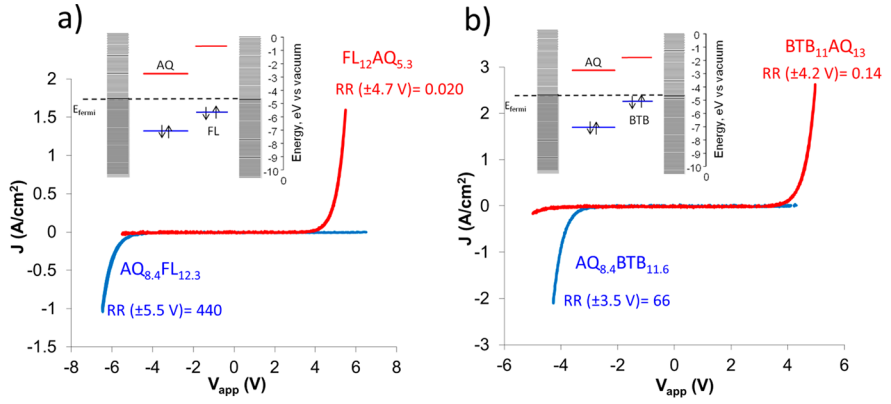

Figure 4. Reversal of the rectification direction with reversing the order of layers in (a) AQ-FL, and (b) AQ-BTB. The insets depict the energy level diagrams of the bilayer components at zero bias, for the case with AQ bonded to PPF in the first layer.

RR = 19 ($V = \pm 2$ V), 58 (±3 V), 148 (±4 V), and 240 (±5 V) for the case of $NDI_{10.7}/BTB_{10.3}$ shown in Figure 3c and 3d. As shown in Figure 3d, an $NDI_{10.7}AQ_{11.9}$ junction has a small rectification ratio (<2 at ±6.2 V), compared to 240 at ±5 V for $NDI_{10.7}BTB_{10.3}$. Note also that all junctions in this comparison have compositionally similar sp^2 carbon contacts, so changes in rectification cannot result from differences in the contact work functions and must result from changes in molecular structure or the molecule/contact interfaces.

To further confirm that the origin of rectification is due to molecular properties and not the contacts or junction structure, additional bilayers were examined. Attempts to change the direction of rectification in the NDI/BTB system by changing the order of the two layers resulted in BTB/NDI devices with low yield and short lifetime, but combinations of AQ with BTB or FL were more successful. Figure 4a shows rectification by an $AQ_{8.4}/FL_{12.3}$ bilayer junction, with RR = 440 at ±5.5 V. As was the case with NDI/BTB, large *J* was observed when the layer containing the stronger electron acceptor (AQ) was biased negative. Also shown in Figure 4a is a $FL_{12}AQ_{5.3}$ device, that has the order of the two layers reversed for which the direction of rectification is also reversed, with RR = 0.020 at ±4.7 V. Note that the larger *J* is still observed when the AQ layer is biased negatively, and rectification direction is determined solely by the order of the layers and the difference in orbital energies. Figure 4b shows a similar comparison for AQ/BTB devices, which also exhibit reversal of the direction of rectification when the order of the layers is reversed. Figure 5a–c compares the NDI/AQ bilayer to NDI/NAB and NDI/FL bilayer junctions, all with total molecular layer thickness in the range of 20–23 nm. Figure 5d–f shows the same data as $|J|$ vs $|V|$ to more readily observe the differences between the positive and negative polarities. Table 3 lists *JV* and RR results for eight bilayer junctions with molecular layer thicknesses in the range of 17–24 nm. The RR was determined in all cases at the applied bias which produced $|J| = 0.2$ A/cm^2, and is always

DOI: 10.1021/jacs.6b07499
J. Am. Chem. Soc. 2016, 138, 12287–12296

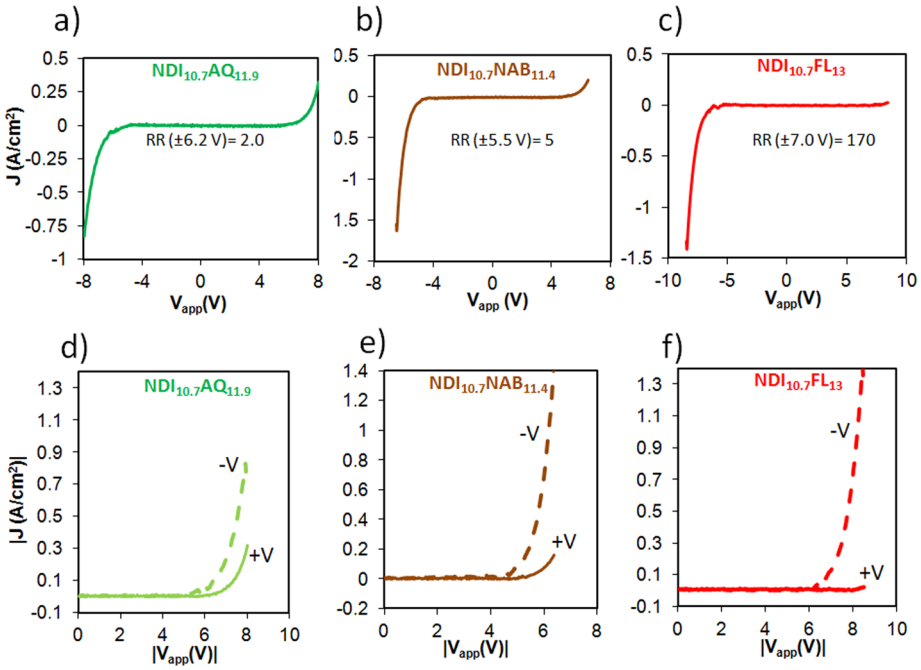

Figure 5. *JV* curves for (a) NDI-AQ, (b). NDI-NAB, and (c) NDI-FL bilayer junctions with the indicated layer thicknesses. To illustrate asymmetry, the same *JV* curves are plotted as the absolute value of current density versus absolute value of bias voltage for (d) NDI-AQ, (e) NDI-NAB, and (f) NDI-FL.

Table 3. Rectification Ratios of Various Bilayer Combinations

bilayer	first layer thickness, nm	second layer thickness, nm	total thickness, nm	V_1 for |J| = 0.2 A/cm^2	J ($-V_1$)	J ($+V_1$)	RSD[a] of J ($-V_1$)	RR ($\pm V_1$)	RR ($\pm V_{max}$)[b]	RSD[a] in RR ($\pm V_{max}$)[c]	# junctions
NDI/BTB	10.7	10.3	21	−3.92	−0.207	0.003	36%	80	240 (±5 V)	39%	25
NDI/AQ	10.7	11.9	22.6	−6.19	−0.199	0.100	14%	2.0	2.5 (±8 V)	21%	4
NDI/NAB	10.7	11.4	22.1	−5.48	−0.206	0.038	16%	5.0	8 (±6.5 V)	28%	4
NDI/FL	10.7	13	23.7	−7.03	−0.200	0.001	9%	170	155 (±8.5 V)	64%	4
AQ/BTB	8.4	11.6	20	−3.55	−0.210	0.003	13%	66.0	95 (±4.5 V)	13%	4
BTB/AQ	11	13	24	4.15	−0.031	0.219	24%[c]	0.140	0.05 (±5 V)	32%	4
AQ/FL	8.4	12.3	20.7	−5.55	−0.210	0.00048	18%	440	290 (±6.5 V)	5%	4
FL/AQ	12	5.3	17.3	4.68	−0.004	0.208	49%[c]	0.020	0.014 (±5.5 V)	38%	6

[a]Relative standard deviation based on the number of junctions indicated in the far right column. [b]RR values at maximum compliance of the instrument. [c]Determined at $+V_1$ due to reversal of rectification

stated as the absolute value of the ratio of J for negative bias to J for positive bias. The RR values less than one correspond to the cases where rectification is reversed from that observed for NDI/BTB (i.e., BTB/AQ and FL/AQ, shown in Figure 4). Table 3 includes the standard deviations of J and RR for at least four junctions of each type as well as the RR observed near the compliance limit of the instrument. In most cases, the RR increased with bias as noted above for NDI/BTB, but in two cases (AQ/FL and NDI/FL) the RR decreased slightly between V_1 and V_{max}, as shown in Table 3.

Charge transport in "bulk" organic semiconductors and redox polymers with layer thickness >100 nm is generally temperature dependent, attributed to various mechanisms such as Marcus-like redox exchange and variable range hopping. Molecular junctions with d < 5 nm are temperature independent, as expected for tunneling transport, notably conjugated examples such as NAB[26] and oligophenylimines.[25,29] The temperature dependence of the $NDI_{10.7}/BTB_{10.3}$ bilayer MJ was examined over the range of 7−320 K in order to provide mechanistic insights, with the results shown in Figure 6 and Table 4.

Figure 6a shows that rectification is maintained at 7 K, and that there is little change in the *JV* response between 7 and 100 K. Arrhenius plots of ln J(−4.5 V) and ln J(+4.5 V) vs $1/T$ in Figure 6c show a gradual change in slope from ∼100 meV at high T to 5−30 meV in the range of 110−140 K. Arrhenius plots for the 7−320 K range in Figure 6d and for a different

DOI: 10.1021/jacs.6b07499
J. Am. Chem. Soc. 2016, 138, 12287−12296

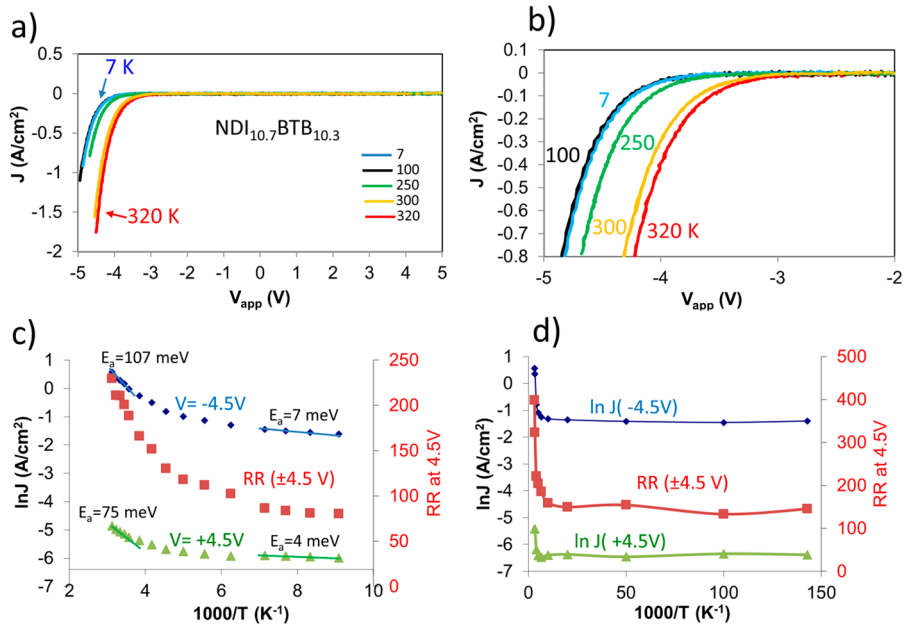

Figure 6. (a) *JV* curves for $NDI_{10.7}BTB_{10.3}$ bilayer junction at indicated temperatures from 7 to 320 K. (b) Magnified plot of −2 to −5 V bias range. (c) ln *J* (left axis) vs $1/T$ at ±4.5 V for a $NDI_{10.7}BTB_{10.3}$ bilayer junction with several Arrhenius slopes indicated. Temperature dependence of RR (±4.5) also shown using right axis. (d). ln *J* and RR for 7 K to 300 K, in same format as (c).

Table 4. Arrhenius Slopes for Indicated Temperature Ranges, All in meV

	bias, V	7−100 K	110−140 K	280−320 K
$NDI_{10.7}/BTB_{10.3}$	+4.5	<0.02	4	75
	+4.0	<0.02	6	79
	+3.5	<0.02	1	123
	+3.0		9	141
	+2.5		14	176
	−2.5		22	272
	−3.0		28	240
	−3.5	0.05	11	196
	−4	<0.02	9	137
	−4.5	0.05	7	107
$NDI_{10.7}$	+3.0		1.8	42
	+2.5		2	56
	+2.0		6.5	44
	−2.0		7.3	31
	−2.5		3.7	54
	−3.0		2	39
BTB22[a]	+4.5	0.15[b]	11.4[c]	19[d]
	+4.0	0.16[b]	14[c]	23[d]
	+3.5		17.4[c]	42[d]
	+3.0		22[c]	47[d]
	+2.5		28[c]	98[d]
	−2.5		25.9[c]	99[d]
	−3.0		12.5[c]	85[d]
	−3.5		20.25[c]	59[d]
	−4.0	0.1[b]	16.89[c]	34[d]
	−4.5	0.09[b]	13.46[c]	25[d]
$BTB_{10.4}$[a]	+2.0	0.1[b]	2[c]	36[d]
	+1.5	0.1[b]	4[c]	54[d]
	+1.0	0.01[b]	5[c]	75[d]

[a]Data from reference 33. [b]5−50 K temperature range. [c]100−200 K. [d]200−300 K.

junction show very weak temperature dependence below 100 K, with Arrhenius slopes statistically indistinguishable from zero. The rectification ratio at ±4.5 V is also plotted in panels c and d, for comparison to the changes in current density. The variation in RR at low T varies from sample to sample presumably due to thickness variations of the two layers, but in all cases the RR for a given MJ was constant with temperature below 100 K.

DISCUSSION

The experimental results permit several conclusions about the effect of molecular energy levels on current voltage response in single component and bilayer molecular junctions. Regarding the single-component layers, we conclude first that conjugated bilayers can support electron transport across molecular layer thicknesses greater than 20 nm, much too far for coherent tunneling, and much farther than transport in alkanes. Transport persists even for temperatures below 10 K, implying that Marcus-type reorganization before electron transport is not a prerequisite for transport and alternatives to coherent tunneling and Marcus transport must be considered.[33] This observation rules out many of the conduction mechanisms reported for thick organic semiconductors, such as activated redox exchange "hopping", which may only contribute at and above room temperature in the current devices. Second, all cases of single-component molecular layers yielded nearly symmetric *JV* response, with RR < 2. Considering NDI and BTB, the single component junctions are symmetric ($BTB_{10.4}$, RR = 1.3; $NDI_{10.7}$, RR = 0.43; BTB_{22}, RR = 0.43, $NDI_{23.9}$, RR = 0.35), while a $NDI_{10.7}/BTB_{10.3}$ bilayer is asymmetric, with RR = 80). We reported previously that 4−22 nm BTB MJs exhibited symmetric *JV* curves,[33] so the *JV* symmetry of single component layers for d > 5 nm was expected. However, the large difference in conductance between $NDI_{10.7}$ and $BTB_{10.4}$ (Figure 1b,c) was not expected if the trend observed for d < 5 nm persisted in thicker MJs. We have reported that aromatic molecular junctions with d = 2−5 nm and a >2 eV variation in

DOI: 10.1021/jacs.6b07499
J. Am. Chem. Soc. 2016, 138, 12287−12296

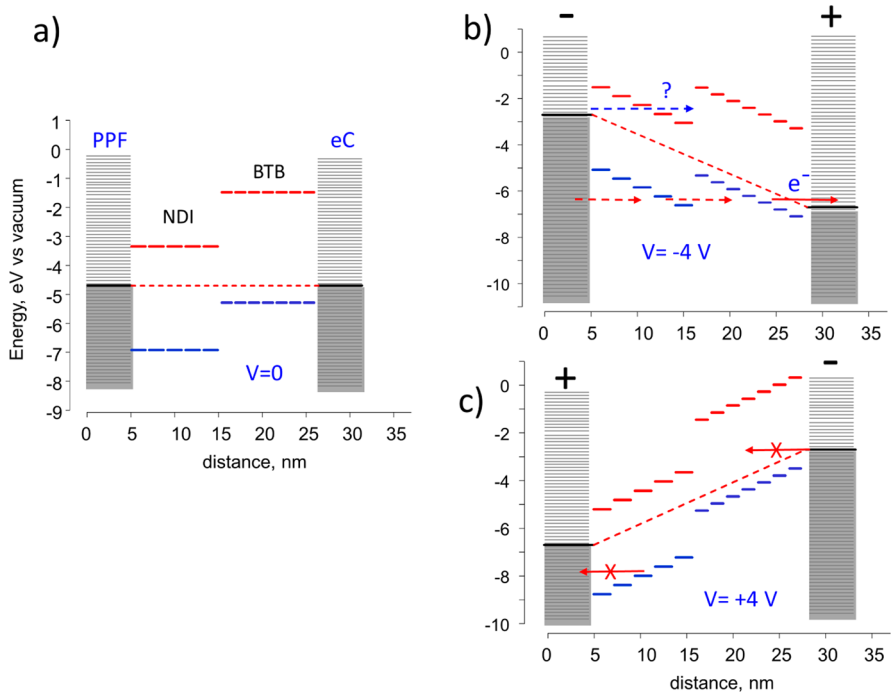

Figure 7. (a) Energy level diagram for a bilayer junction of five NDI molecules and seven BTB molecules, to approximate the $NDI_{10.7}BTB_{10.3}$ bilayer junction at zero bias, using free-molecule DFT energies and a PPF Fermi level of −4.7 eV. (b) the same diagram with a −4 V bias (PPF negative), assuming a linear potential profile through the molecular layers. (c) same diagram for +4 V bias. Arrows indicate possible electron transfers between contacts and molecular layers (see text for explanation).

HOMO and LUMO energies had very similar *JV* behavior, in both magnitude and dependence on thickness.[27] The weak effect of orbital energies on *JV* response was attributed to strong electronic coupling between the carbon contacts and the aromatic molecules, which causes deviation from classical Mott−Schottky behavior. This coupling has a "leveling" effect (or "vacuum level shift") which is known to occur at metal/organic interfaces.[31,73,74] However, for $d \geq 7$ nm, single-component layers of NDI and BTB current densities differ by orders of magnitude (Figure 1b), as do NDI, BTB, azobenzene and NAB devices used for light emission experiments.[61] An important conclusion about single-component MJs from these observations is that molecular structure and presumably orbital energies have pronounced effects on *JV* behavior for aromatic MJs with $d > 5$ nm. This result is reasonable if the strong coupling effect is limited to ∼5 nm from the conducting carbon surface in aromatic devices, and current research on this possibility is in progress.

As noted in the introduction, the *JV* response for bilayers with total thickness <5 nm did not differ significantly from single-component MJs, even for substantial structural and orbital energy differences.[60] Thicker bilayers of molecules with similar HOMO and LUMO energies ($NDI_{10.7}$ and $AQ_{11.9}$) and similar thickness to $NDI_{10.7}/BTB_{10.3}$ exhibit small asymmetry (RR = 2). The NDI/AQ bilayer with a total thickness of 22.5 nm (Figure 3d) and a 24 nm NDI single-component MJ (Figure S7b) have similar symmetry (RR ≤ 2). However, significant asymmetry (RR > 10) occurs when both the HOMO and LUMO energies of the two component layers differ by more than 1 eV. In all cases where RR > 10, involving eight different bilayer combinations, the larger current of the asymmetric *JV* curve occurs when the stronger electron donor (i.e., higher HOMO energy) is positively biased and the stronger electron acceptor (lower LUMO energy) is negatively biased. Asymmetry was decreased significantly (RR < 10) for NDI/BTB if one or both of the two layers was thinner than 6 nm (Table 2). At least for the range of bilayer combinations studied, large RR required both layers to be ∼10 nm, although there is likely room for further optimization. Finally, the RR for NDI/BTB decreases with decreasing temperature by a factor of 2−3 between 300 and 7 K, but is still large at 7K (∼150 in Figure 6d). The RR is nearly constant and the Arrhenius slopes are statistically zero from 7 to 100 K, indicating that activation or reorganization before electron transfer are not important for transport and rectification at low temperature. The increases of the observed Arrhenius slope above 100 K could arise from several effects, including Fermi function[26] or molecular energy level broadening or activated redox exchange,[33] but neither effect is required for the observed rectification.

These observations clearly demonstrate that orbital energies can determine electronic behavior, and that a rectifying molecular junction can be "designed" on the basis of differences in HOMO and LUMO energies. This conclusion represents one example of the "molecular signature" often sought in molecular electronics, in which electronic behavior can be altered, perhaps systematically, by changes in molecular structure. The mechanism underlying the effect of orbital energies on *JV* symmetry may be considered starting with the diagram of Figure 7a, which shows the Fermi levels and orbital energies for a NDI/BTB bilayer junction containing five NDI molecules and seven BTB molecules, for idealized layer thicknesses of 10.3 and 11.0 nm to approximate the devices with the observed *JV* behavior shown in Figure 1. The dashed red line indicates the potential profile for the simplest case of a constant electric field across a dielectric material under bias. As already noted, breakdown of the Mott−Schottky approximation may perturb the field and energy distributions near the

DOI: 10.1021/jacs.6b07499
J. Am. Chem. Soc. 2016, 138, 12287−12296

contacts, but the diagram ignores that effect for simplicity. The weak temperature dependence of both J and RR, particularly below 200 K, indicates that thermal population of the LUMO or Marcus-like reorganization before electron transfer are unlikely to be involved significantly in transport. As shown in Figure 7b, the high electric field under bias (~2 MV/cm for V = −4 V), is predicted to cause significant shifts in orbital energies due to the linear potential profile altering the local electrostatic potential of each molecule in the bilayer. A bias of −4 V (with PPF negative) could raise the HOMO energies of molecules close to the eC contact and permit transport from a HOMO into empty eC orbitals, as indicated by the solid red arrow in 7B. Such transport could be by tunneling or field ionization,[33] but in either case the distance is much shorter than the 21 nm bilayer thickness. One possibility for continued transport is shown by the dashed red arrows, with the net result being transport from PPF to eC through the molecular HOMOs. The opposite bias of +4 V as shown in Figure 7c indicates a quite different situation. Electrons in the NDI HOMO cannot transfer into the filled PPF orbitals, nor can electrons in eC reach empty BTB orbitals. Note that this simple model relies only on the differences in frontier orbital energies of the molecular layers, since the Fermi levels of the carbon contacts are nominally equal. Therefore, bilayers made from two molecules with similar HOMO and LUMO energies (e.g., NDI/AQ) yield nearly symmetric JV response, while reversing the order of the two layers in AQ/FL or AQ/BTB causes reversal of the direction of rectification.

As already noted, in all rectifying bilayers (with RR > 10), the larger junction current was observed when the stronger electron acceptor was biased negative and the stronger donor was biased positive. The concept of "injection" often used in organic electronics applies to the current devices, but with some limitations. The higher currents correspond to the lower "injection" barriers for the rectifiers, but this process is not thermally activated, and can occur at either PPF or eC interfaces with the bilayer. Asymmetry is not the result of different contact work functions, as is often the case for organic p−n junctions with much thicker layers. "Injection" in the current devices is likely field driven and operative even at low temperature, with RR constant from 7 to 200 K. Previous reports based on transport[26] and photocurrents[63,75] indicated that transport in several aromatic carbon-based MJs with d < 5 nm is hole mediated, meaning the important barrier is that between the molecular HOMO and the contact Fermi level. An exception is NDI, which exhibits photocurrents consistent with LUMO mediation.[63] While the observed RR roughly correlates with the HOMO to Fermi Level offset, it also does to the LUMO to E_f offset. Figure 7b also shows an electron transported from PPF to the NDI LUMO (dashed blue arrow), resulting in similar rectification. The current results clearly indicate that molecular structure and orbital energies can affect the electronic behavior of bilayer molecular junctions, but additional examples are necessary to identify which orbitals are involved. In addition, the mechanism of Figure 7 applies to bilayers which are made entirely from conjugated molecules, and lack the mix of aliphatic and aromatic components in which rectification is observed in alkyl ferrocene molecular junctions.[15,17,40] The larger variation in orbital energies and dielectric constant of the latter devices may result in a quite different rectification mechanism.

In conclusion, the results provide a "molecular signature" that exhibits significant changes in electronic behavior with variation of molecular structure. In all cases studied, the molecular layers were thicker than the approximately 5 nm over which strong electronic coupling with the carbon contact is observed, where the aforementioned "leveling" effect decreases the effect of orbital energy variation.[27] While the rectification direction is similar to that observed for much thicker organic "p−n" junctions, the mechanism does not involve the same "injection" present in organic light emitting diodes, and it does not require contacts with different work functions. As is likely also the case for unimolecular rectifiers, the nanoscale transport distances and high electric fields of the current devices enable transport mechanisms not operative in conventional organic electronics in films with thicknesses greater than 100 nm.

■ ASSOCIATED CONTENT

Supporting Information

The Supporting Information is available free of charge on the ACS Publications website at DOI: 10.1021/jacs.6b07499.

Junction fabrication details, optical and XPS spectra, and additional JV curves (PDF)

■ AUTHOR INFORMATION

Corresponding Author

*mccreery@ualberta.ca

Notes

The authors declare no competing financial interest.

■ ACKNOWLEDGMENTS

This work was supported by the University of Alberta, the National Research Council of Canada, the National Science and Engineering Research Council and Alberta Innovates. ANR (France) is gratefully acknowledged for its financial support of this work (ANR-15-CE09 0001-01). We thank Mykola Kondratenko for NDI synthesis, Amin Morteza-Najarian for AQ and FL diazonium synthesis and Bryan Szeto for expert assistance with LabView programming and device fabrication.

■ REFERENCES

(1) Xiang, D.; Wang, X.; Jia, C.; Lee, T.; Guo, X. *Chem. Rev.* **2016**, *116*, 4318−4440.
(2) Metzger, R. M. *Chem. Rev.* **2015**, *115*, 5056−5115.
(3) McCreery, R.; Yan, H.; Bergren, A. J. *Phys. Chem. Chem. Phys.* **2013**, *15*, 1065−1081.
(4) Amdursky, N.; Marchak, D.; Sepunaru, L.; Pecht, I.; Sheves, M.; Cahen, D. *Adv. Mater.* **2014**, *26*, 7142−7161.
(5) Yoon, H. J.; Shapiro, N. D.; Park, K. M.; Thuo, M. M.; Soh, S.; Whitesides, G. M. *Angew. Chem., Int. Ed.* **2012**, *51*, 4658−4661.
(6) Dickey, M. D.; Chiechi, R. C.; Larsen, R. J.; Weiss, E. A.; Weitz, D. A.; Whitesides, G. M. *Adv. Funct. Mater.* **2008**, *18*, 1097−1104.
(7) Tran, E.; Duati, M.; Mullen, K.; Zharnikov, M.; Whitesides, G. M.; Rampi, M. *Adv. Mater.* **2006**, *18*, 1323.
(8) Bowers, C. M.; Zhang, M.; Lyubarskaya, Y.; Toone, E. J.; Tang, C.; Shestopalov, A. A. *Adv. Mater. Interfaces* **2014**, *1*, 1300109.
(9) Finklea, H. O. Electrochemistry of Organized Monolayers of Thiols and Related Molecules on Electrodes. In *Electroanalytical Chemistry*; Bard, A. J., Ed.; Dekker: New York, 1996; Vol. *19*, pp 109−335.
(10) Finklea, H. O.; Hanshew, D. D. *J. Am. Chem. Soc.* **1992**, *114*, 3173−3181.
(11) Smalley, J. F.; Finkea, H. O.; Chidsey, C. E. D.; Linford, M. R.; Creager, S. E.; Ferraris, J. P.; Chalfant, K.; Zawodzinsk, T.; Feldberg, S. W.; Newton, M. D. *J. Am. Chem. Soc.* **2003**, *125*, 2004−2013.
(12) Smalley, J. F.; Feldberg, S. W.; Chidsey, C. E. D.; Linford, M. R.; Newton, M. D.; Liu, Y.-P. *J. Phys. Chem.* **1995**, *99*, 13141−13149.

DOI: 10.1021/jacs.6b07499
J. Am. Chem. Soc. 2016, 138, 12287−12296

(13) Chidsey, C. E. D. *Science* **1991**, *251*, 919−923.
(14) Polo, F.; Antonello, S.; Formaggio, F.; Toniolo, C.; Maran, F. *J. Am. Chem. Soc.* **2004**, *127*, 492−493.
(15) Yuan, L.; Nerngchamnong, N.; Cao, L.; Hamoudi, H.; del Barco, E.; Roemer, M.; Sriramula, R. K.; Thompson, D.; Nijhuis, C. A. *Nat. Commun.* **2015**, *6*, 7324.
(16) Yuan, L.; Breuer, R.; Jiang, L.; Schmittel, M.; Nijhuis, C. A. *Nano Lett.* **2015**, *15*, 5506−5512.
(17) Nijhuis, C. A.; Reus, W. F.; Whitesides, G. M. *J. Am. Chem. Soc.* **2009**, *131*, 17814−17827.
(18) Chabinyc, M. L.; Chen, X.; Holmlin, R.; Jacobs, H.; Skulason, H.; Frisbie, C. D.; Mujica, V.; Ratner, M.; Rampi, M. A.; Whitesides, G. M. *J. Am. Chem. Soc.* **2002**, *124*, 11730−11736.
(19) Hihath, J.; Bruot, C.; Nakamura, H.; Asai, Y.; Díez-Pérez, I.; Lee, Y.; Yu, L.; Tao, N. *ACS Nano* **2011**, *5*, 8331−8339.
(20) Yoon, H. P.; Maitani, M. M.; Cabarcos, O. M.; Cai, L.; Mayer, T. S.; Allara, D. L. *Nano Lett.* **2010**, *10*, 2897−2902.
(21) Leng, J.-C.; Lin, L. L.; Song, X.-N.; Li, Z.-L.; Wang, C.-K. *J. Phys. Chem. C* **2009**, *113*, 18353−18357.
(22) Yu, L. H.; Zangmeister, C. D.; Kushmerick, J. G. *Phys. Rev. Lett.* **2007**, *98*, 206803−206804.
(23) Honciuc, A.; Metzger, R. M.; Gong, A.; Spangler, C. W. *J. Am. Chem. Soc.* **2007**, *129*, 8310−8319.
(24) Luo, L.; Choi, S. H.; Frisbie, C. D. *Chem. Mater.* **2011**, *23*, 631−645.
(25) Choi, S. H.; Kim, B.; Frisbie, C. D. *Science* **2008**, *320*, 1482−1486.
(26) Bergren, A. J.; McCreery, R. L.; Stoyanov, S. R.; Gusarov, S.; Kovalenko, A. *J. Phys. Chem. C* **2010**, *114*, 15806−15815.
(27) Sayed, S. Y.; Fereiro, J. A.; Yan, H.; McCreery, R. L.; Bergren, A. J. *Proc. Natl. Acad. Sci. U. S. A.* **2012**, *109*, 11498−11503.
(28) Xie, Z.; Bâldea, I.; Smith, C. E.; Wu, Y.; Frisbie, C. D. *ACS Nano* **2015**, *9*, 8022−8036.
(29) Kim, B.; Choi, S. H.; Zhu, X. Y.; Frisbie, C. D. *J. Am. Chem. Soc.* **2011**, *133*, 19864−19877.
(30) Yaffe, O.; Qi, Y. B.; Scheres, L.; Puniredd, S. R.; Segev, L.; Ely, T.; Haick, H.; Zuilhof, H.; Vilan, A.; Kronik, L.; Kahn, A.; Cahen, D. *Phys. Rev. B: Condens. Matter Mater. Phys.* **2012**, *85*, 045433.
(31) Vilan, A.; Yaffe, O.; Biller, A.; Salomon, A.; Kahn, A.; Cahen, D. *Adv. Mater.* **2010**, *22*, 140−159.
(32) Cahen, D.; Kahn, A. *Adv. Mater.* **2003**, *15*, 271−277.
(33) Yan, H.; Bergren, A. J.; McCreery, R.; Della Rocca, M. L.; Martin, P.; Lafarge, P.; Lacroix, J. C. *Proc. Natl. Acad. Sci. U. S. A.* **2013**, *110*, 5326−5330.
(34) Choi, S. H.; Risko, C.; Delgado, M. C. R.; Kim, B.; Bredas, J.-L.; Frisbie, C. D. *J. Am. Chem. Soc.* **2010**, *132*, 4358−4368.
(35) Aviram, A.; Ratner, M. *Chem. Phys. Lett.* **1974**, *29*, 277−283.
(36) Elbing, M.; Ochs, R.; Koentopp, M.; Fischer, M.; von Hänisch, C.; Weigend, F.; Evers, F.; Weber, H. B.; Mayor, M. *Proc. Natl. Acad. Sci. U. S. A.* **2005**, *102*, 8815−8820.
(37) Stadler, R.; Geskin, V.; Cornil, J. *J. Phys.: Condens. Matter* **2008**, *20*, 374105.
(38) Berlin, Y. A.; Grozema, F. C.; Siebbeles, L. D. A.; Ratner, M. A. *J. Phys. Chem. C* **2008**, *112*, 10988−11000.
(39) Nijhuis, C. A.; Reus, W. F.; Siegel, A. C.; Whitesides, G. M. *J. Am. Chem. Soc.* **2011**, *133*, 15397−15411.
(40) Nijhuis, C. A.; Reus, W. F.; Whitesides, G. M. *J. Am. Chem. Soc.* **2010**, *132*, 18386−18401.
(41) Van Dyck, C.; Ratner, M. A. *Nano Lett.* **2015**, *15*, 1577−1584.
(42) Fluteau, T.; Bessis, C.; Barraud, C.; Della Rocca, M. L.; Martin, P.; Lacroix, J.-C.; Lafarge, P. *J. Appl. Phys.* **2014**, *116*, 114509.
(43) Martin, P.; Della Rocca, M. L.; Anthore, A.; Lafarge, P.; Lacroix, J.-C. *J. Am. Chem. Soc.* **2012**, *134*, 154−157.
(44) Kuikka, M. A.; Li, W.; Kavanagh, K. L.; Yu, H.-Z. *J. Phys. Chem. C* **2008**, *112*, 9081−9088.
(45) Zhao, J.; Yu, C.; Wang, N.; Liu, H. *J. Phys. Chem. C* **2010**, *114*, 4135−4141.
(46) Capozzi, B.; Xia, J.; Adak, O.; Dell, E. J.; Liu, Z.-F.; Taylor, J. C.; Neaton, J. B.; Campos, L. M.; Venkataraman, L. *Nat. Nanotechnol.* **2015**, *10*, 522−527.
(47) Zhang, W.; Zhang, X.; Lu, C.; Wang, Y.; Deng, Y. *J. Phys. Chem. C* **2012**, *116*, 9227−9234.
(48) Jin, Y.; Friedman, N.; Sheves, M.; Cahen, D. *Langmuir* **2008**, *24*, 5622−5626.
(49) Yu, X.; Lovrinčić, R.; Kraynis, O.; Man, G.; Ely, T.; Zohar, A.; Toledano, T.; Cahen, D.; Vilan, A. *Small* **2014**, *10*, 5151−5160.
(50) Li, Y.; Calder, S.; Yaffe, O.; Cahen, D.; Haick, H.; Kronik, L.; Zuilhof, H. *Langmuir* **2012**, *28*, 9920−9929.
(51) Popoff, R. T. W.; Zavareh, A. A.; Kavanagh, K. L.; Yu, H.-Z. *J. Phys. Chem. C* **2012**, *116*, 17040−17047.
(52) Popoff, R. T. W.; Asanuma, H.; Yu, H.-Z. *J. Phys. Chem. C* **2010**, *114*, 10866−10872.
(53) Zhu, L.; Popoff, R. T. W.; Yu, H.-Z. *J. Phys. Chem. C* **2015**, *119*, 1826−1831.
(54) Kleemann, H.; Gutierrez, R.; Avdoshenko, S.; Cuniberti, G.; Leo, K.; Lüssem, B. *Org. Electron.* **2013**, *14*, 193−199.
(55) Kleemann, H.; Gutierrez, R.; Lindner, F.; Avdoshenko, S.; Manrique, P. D.; Lulssem, B. r.; Cuniberti, G.; Leo, K. *Nano Lett.* **2010**, *10*, 4929−4934.
(56) Sengoku, T.; Yamao, T.; Hotta, S. *J. Non-Cryst. Solids* **2012**, *358*, 2525−2529.
(57) Saracco, E.; Bouthinon, B.; Verilhac, J.-M.; Celle, C.; Chevalier, N.; Mariolle, D.; Dhez, O.; Simonato, J.-P. *Adv. Mater.* **2013**, *25*, 6534−6538.
(58) Kong, H.; Sinha, J.; Hoeft, D.; Kirschner, S. B.; Reich, D. H.; Katz, H. E. *Org. Electron.* **2013**, *14*, 703−710.
(59) Gong, X.; Tong, M.; Xia, Y.; Cai, W.; Moon, J. S.; Cao, Y.; Yu, G.; Shieh, C.-L.; Nilsson, B.; Heeger, A. J. *Science* **2009**, *325*, 1665−1667.
(60) Sayed, S. Y.; Bayat, A.; Kondratenko, M.; Leroux, Y.; Hapiot, P.; McCreery, R. L. *J. Am. Chem. Soc.* **2013**, *135*, 12972−12975.
(61) Ivashenko, O.; Bergren, A. J.; McCreery, R. L. *J. Am. Chem. Soc.* **2016**, *138*, 722−725.
(62) Yan, H.; Bergren, A. J.; McCreery, R. L. *J. Am. Chem. Soc.* **2011**, *133*, 19168−19177.
(63) Fereiro, J. A.; Kondratenko, M.; Bergren, A. J.; McCreery, R. L. *J. Am. Chem. Soc.* **2015**, *137*, 1296−1304.
(64) Fave, C.; Leroux, Y.; Trippe, G.; Randriamahazaka, H.; Noel, V.; Lacroix, J.-C. *J. Am. Chem. Soc.* **2007**, *129*, 1890−1891.
(65) Santos, L.; Ghilane, J.; Lacroix, J. C. *J. Am. Chem. Soc.* **2012**, *134*, 5476−5479.
(66) Anariba, F.; DuVall, S. H.; McCreery, R. L. *Anal. Chem.* **2003**, *75*, 3837−3844.
(67) Hurley, B. L.; McCreery, R. L. *J. Electrochem. Soc.* **2004**, *151*, B252.
(68) Belanger, D.; Pinson, J. *Chem. Soc. Rev.* **2011**, *40*, 3995−4048.
(69) Stockhausen, V.; Trippé-Allard, G.; Van Quynh, N.; Ghilane, J.; Lacroix, J.-C. *J. Phys. Chem. C* **2015**, *119*, 19218−19227.
(70) Bergren, A. J.; McCreery, R. L. *Annu. Rev. Anal. Chem.* **2011**, *4*, 173−195.
(71) Ru, J.; Szeto, B.; Bonifas, A.; McCreery, R. L. *ACS Appl. Mater. Interfaces* **2010**, *2*, 3693−3701.
(72) Anariba, F.; Viswanathan, U.; Bocian, D. F.; McCreery, R. L. *Anal. Chem.* **2006**, *78*, 3104−3112.
(73) Hwang, J.; Wan, A.; Kahn, A. *Mater. Sci. Eng., R* **2009**, *64*, 1−31.
(74) Braun, S.; Salaneck, W. R.; Fahlman, M. *Adv. Mater.* **2009**, *21*, 1450−1472.
(75) Fereiro, J. A.; McCreery, R. L.; Bergren, A. J. *J. Am. Chem. Soc.* **2013**, *135*, 9584−9587.

DOI: 10.1021/jacs.6b07499
J. Am. Chem. Soc. 2016, 138, 12287−12296